

Analytical and Numerical study of the out-of-equilibrium current through a helical edge coupled to a magnetic impurity

Yuval Vinkler-Aviv,¹ Daniel May,² and Frithjof B. Anders²

¹*University of Cologne, Institute for Theoretical Physics, 50937 Cologne, Germany*

²*Theoretische Physik 2, Technische Universität Dortmund, 44221 Dortmund, Germany*

We study the conductance of a time-reversal symmetric helical electronic edge coupled anti-ferromagnetically to a magnetic impurity, employing analytical and numerical approaches. The impurity can reduce the perfect conductance G_0 of a noninteracting helical edge by generating a backscattered current. The backscattered steady-state current tends to vanish below the Kondo temperature T_K for time-reversal symmetric setups. We show that the central role in maintaining the perfect conductance is played by a global $U(1)$ symmetry. This symmetry can be broken by an anisotropic exchange coupling of the helical modes to the local impurity. Such anisotropy, in general, dynamically vanishes during the renormalization group (RG) flow to the strong coupling limit at low-temperatures. The role of the anisotropic exchange coupling is further studied using the time-dependent Numerical Renormalization Group (TD-NRG) method, uniquely suitable for calculating out-of-equilibrium observables of strongly correlated setups. We investigate the role of finite bias voltage and temperature in cutting the RG flow before the isotropic strong-coupling fixed point is reached, extract the relevant energy scales and the manner in which the crossover from the weakly interacting regime to the strong-coupling backscattering-free screened regime is manifested. Most notably, we find that at low temperatures the conductance of the backscattering current follows a power-law behavior $G \sim (T/T_K)^2$, which we understand as a strong nonlinear effect due to time-reversal symmetry breaking by the finite-bias.

I. INTRODUCTION

Chiral electronic channels, which can be found on the edges of an integer quantum Hall sample, show unique conductance behavior. As backscattering of electrons is not possible, the conductance of these channels is robust against many perturbations, *inter alia* scattering off impurities, and it attains the universal value of $G_0 = e^2/h$ per charge-carrying channel. While a system with a single chirality requires breaking of time-reversal symmetry, as in the quantum Hall effect, a more nuanced picture emerges when one considers helical modes. In these systems, the spin and propagation direction are interlinked, with opposite flavors of spins counter-propagating. For example, the edges of a topological insulator such as a quantum spin-Hall bar demonstrate this behavior, without breaking time-reversal symmetry [1–4]. Such systems have focused a great amount of interest in recent years, both experimentally and theoretically. One of the signatures of the quantum spin-Hall state should be a perfect edge conductance at low temperatures and bias voltages when time-reversal symmetry is maintained, as backscattering of electrons along the edge requires flipping of the spin, which is strongly suppressed in presence of time-reversal symmetry.

Experimentally, however, the perfect quantization of the conductance was not observed, despite measurements in different topological insulators such as HgTe/CdTe and InAs/GaSb quantum wells, bismuth layers and WTe₂ monolayers [5–24]. Suggestions for the potential sources for the deviation from perfect conductance include effects such as electron-electron interactions, disorder, electrical noise, inelastic scattering, and others [25–35].

The question of the effect of magnetic impurities on the

conductance along helical edges was the subject of theoretical attention as well, considering different forms of impurities, coupling, and electronic band structures [36–50]. At low temperatures and in the absence of strong electron-electron interactions, a generic magnetic impurity forms a Kondo singlet and is screened out, allowing the helical edge to reconstitute itself around it and, therefore, has no effect on the conductance. This has been the fundamental picture established by Wu and collaborators and by Maciejko and collaborators [44, 51]. However, identifying the leading corrections at finite temperatures to the perfect conductance is an ongoing subject for debate.

In Ref. [44], the authors employed bosonization and analytical perturbative RG calculations in order to study the backscattering from a magnetic impurity, and predicted that at low temperatures the deviation from perfect conductance scales as $G \propto (T/T_K)^{2(4K-1)}$ as long as $K > 1/4$, where K is the Luttinger parameter describing the strength of the electron-electron interactions along the edge, and T_K the Kondo temperature. Specifically, for noninteracting electrons ($K = 1$), $G \propto (T/T_K)^6$ is found. Väyrynen and collaborators [30] studied the conductance in presence of charge puddles created by disorder and modeled by a series of interacting quantum dots. They reported a deviation from perfect conductance in the linear bias voltage regime and for low temperatures due to a backscattering current with a conductance behavior of $G \propto T^4$. Recently, Kurilovich and collaborators considered coupling to an impurity spin with $S > 1/2$, and focused on the effect of the local spin anisotropy on the conductance [48, 50]. They discovered that this effect is strongly dependent on whether the spins is integer or half-integer, and that the correction is almost tempera-

ture independent down to low temperatures.

As Tanaka and collaborators [52] argued, the isotropic Kondo coupling alone does not affect the perfect dc conductance for any K and temperature T . They showed that this can be understood due to the fact that time-reversal symmetry allows backscattering only accompanied with a spin-flip of the impurity, which can be further flipped back only with backscattering in the opposite direction, thus prohibiting a steady-state backscattered current. In order to circumvent this limitation while preserving time-reversal symmetry, one has to consider an anisotropic exchange coupling [41, 48–50] or describe coupling to a many-level interacting quantum dot [30, 43, 46].

While a plethora of theoretical tools was employed to study the effects of magnetic impurities on the conductance in helical systems, to the best of our knowledge the problem was not yet addressed using advanced numerical tools, despite the large success of such methods, *e.g.* the numerical renormalization group (NRG), in exploring the features of strongly-correlated impurity models [53]. In this paper we employ the NRG and time-dependent NRG (TD-NRG) technique to study the conductance of a helical edge coupled to an impurity in non-equilibrium steady state, when finite bias voltage is applied, over a range of temperatures and exchange couplings.

The structure of the paper is as follows. We start in Sec. II by presenting the model Hamiltonian, deriving the expressions for the current in terms of the non-equilibrium Green's functions of a local degree of freedom and analyze its character. In Sec. III we employ perturbative RG methods to analytically study the structure of the correlations and how they affect the conductance. Then, in Sec. IV, we turn to the advanced numerical method of TD-NRG to calculate the current through the helical modes for different temperatures, bias voltages, and interactions. Finally, in Sec. V we discuss our results and their implications.

II. MODEL AND OBSERVABLES

A. The Hamiltonian and its symmetries

We consider the 1d edge of a quantum spin-Hall insulator, which is characterized by two counter-propagating helical electronic modes, associated with two opposite spin projections and described by the field operators $\psi_\sigma(x)$. The edge electrons are coupled at the origin $x = 0$ to a set of local fermionic degrees of freedom $D_{n,\sigma}$ which describes a local interacting impurity. For the time being, we will not consider specific interaction terms, and discuss the setup in general. The only requirement we shall impose is that the entire setup is time-reversal symmetric, which is satisfied by the helical modes as long as ψ_σ and $\psi_{-\sigma}$ are a Kramers pair, and that they accordingly couple to Kramers pairs degrees of freedom of the impurity.

In reality, the helicity in the edge of quantum spin-Hall insulator comes from spin-orbit coupling, which means that although the left- and right-moving electrons have opposite spin projections at each point, that spin projection is not constant along the edge. This was suggested as a possible backscattering mechanism, allowing for momenta-dependent flipping of the spin through inelastic scattering processes or the Dyakonov-Perel spin relaxation mechanism [27, 54]. As we are interested in the effects of the impurity on the conductance, we neglect this effect and assume that the spin orientation is constant along the edge. This can be formally achieved by applying a space dependent unitary transformation that rotates the spins at each point to the same direction, and then omitting the extra momenta-dependent terms that result from this transformation.

The Hamiltonian that describes the dynamics of the edge electrons is given by

$$\mathcal{H}_e = -iv_F \sum_\sigma \sigma \int dx \psi_\sigma^\dagger(x) \partial_x \psi_\sigma(x), \quad (1)$$

with $\sigma = +1$ ($\sigma = -1$) for right (left) movers, which also have opposite spins. For convenience, and without loss of generality, we shall henceforth identify the right-movers with up-spins in the z -directions and left-movers with down-spins. Under time-reversal transformation \hat{T} , the fields undergo $\hat{T}\psi_\sigma\hat{T}^{-1} = \sigma\psi_{-\sigma}$.

At the origin $x = 0$, the edge electrons hybridize with the degrees of freedom of a local impurity $D_{n,\sigma}$, which might have more than one level (orbital) per spin

$$\mathcal{H}_t = \sum_{\sigma,n} t_{\sigma,n} \psi_\sigma^\dagger(0) D_{n,\sigma} + \text{h.c.}, \quad (2)$$

where $n = 1, \dots, N$ labels the impurity levels, and $t_{n,\sigma}$ the hybridization parameters. The levels of the impurity are also arranged in time-reversal symmetric pairs $\hat{T}D_{n,\sigma}\hat{T}^{-1} = \sigma D_{n,-\sigma}$, where the time-reversal symmetry enforces $t_{n,\sigma} = t_{n,-\sigma}^*$. It is convenient to define a single degree of freedom d_σ with which each spin-flavor of the edge electrons hybridize

$$d_\sigma = t_\sigma^{-1} \sum_n t_{n,\sigma} D_{n,\sigma} \quad (3)$$

with $t_\sigma = \sqrt{\sum_n |t_{n,\sigma}|^2}$, and construct an orthogonal set describing all the other $N - 1$ levels $D_{n,\sigma}^o$. Then

$$\mathcal{H}_t = \sum_\sigma t_\sigma \psi_\sigma^\dagger(0) d_\sigma + \text{h.c.} \quad (4)$$

In the general case where the D -levels are non-degenerate, this transformation leads to extra terms between the impurity levels themselves.

The dynamics of the impurity degrees of freedom, and of potentially other local degrees of freedom that interact with the $D_{n,\sigma}$ orbitals, are described by a general interacting Hamiltonian H_D , which does not contain ψ_σ , and does not violate time-reversal symmetry. The full

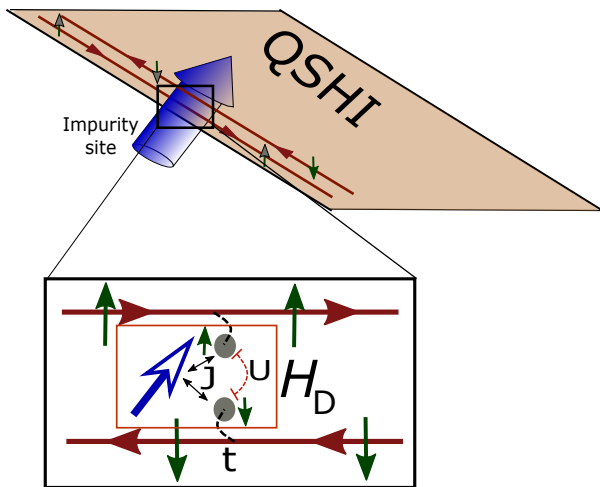


FIG. 1. Schematic depiction of the setup considered throughout most of this paper. A 1d helical edge of a quantum spin Hall insulator consists of right-moving up-spin electrons and left-moving down-spin electrons, coupled at a single point to an generalized impurity via tunnel amplitude t . This impurity encompasses a correlated spinful level interacting with an additional $S = 1/2$ quantum spin. Time reversal symmetry is maintained by making the up and down levels Kramers partners, and keeping a real exchange coupling elements J with the impurity spin.

Hamiltonian is $\mathcal{H} = \mathcal{H}_e + \mathcal{H}_t + \mathcal{H}_D$, and by construction it is time-reversal symmetric. A schematic depiction of the setup is given in Fig. 1, where we assumed energy degenerate impurity orbitals.

B. Electric current

In this section we derive the relevant Meir-Wingreen expression [55] for the electrical current through the edge in terms of the local Green's functions of the localized level d_σ . We analyze its properties and compare it with the expression for the current through a non-helical 1d system.

In absence of a coupling to the localized level, $t_\sigma = 0$, the number of right-moving electrons \hat{N}_R and left-moving electrons \hat{N}_L is constant, and the steady-state current is given by the difference in the corresponding densities $\hat{I}_0 = v_F e (\hat{n}_R - \hat{n}_L)$ with $\hat{n}_{R/L}$ the densities of the left and right movers. Plugging in the density of states per unit length $\rho_0 = 1/(2\pi v_F)$ and integrating over the different occupancies we arrive at the standard result

$$I_0 = \langle \hat{I}_0 \rangle = e \int \frac{d\epsilon}{2\pi} [f(\epsilon - \mu_+) - f(\epsilon - \mu_-)] \quad (5)$$

$$\simeq G_0 \frac{\mu_+ - \mu_-}{e}$$

with μ_\pm the chemical potential of the left and right movers, $f(\epsilon)$ the Fermi-Dirac distribution, and we assumed a large electronic bandwidth $D \gg |\mu_\pm|, T$. The

perfect conduction of the clean channel may be reduced by a backscattered current \hat{I}_B that takes a right moving particle and reflects it into a left moving one $\hat{I} = \hat{I}_0 - \hat{I}_B$. The symmetric form of the backscattered current operator is given by

$$\hat{I}_B = \frac{e}{2} \frac{d}{dt} (\hat{N}_L - \hat{N}_R) \quad (6)$$

$$= i \frac{e}{2} [t_- \psi_-^\dagger(0) d_- - t_+ \psi_+^\dagger(0) d_+ - \text{h.c.}].$$

In order to evaluate $I_B = \langle \hat{I}_B \rangle$ at steady-state, we express it using the lesser Green's functions $G_{AB}^<(\tau, \tau') = \langle B(\tau') A(\tau) \rangle$ which are functions only of the time difference $\tau - \tau'$ at steady-state. Upon Fourier transforming with respect to the time difference we arrive at

$$I_B = e \Im \int \frac{d\omega}{2\pi} [t_+ G_{d_+ \psi_+^\dagger}^<(\omega) - t_- G_{d_- \psi_-^\dagger}^<(\omega)], \quad (7)$$

and by applying standard diagrammatic expansion we obtain

$$G_{d_\sigma \psi_\sigma^\dagger}^<(\omega) = t_\sigma^* [G_{d_\sigma d_\sigma^\dagger}(\omega) g_{\psi_\sigma \psi_\sigma^\dagger}(\omega)]^<.$$

Here $g(\omega)$ is the bare Green's function taken with respect to \mathcal{H}_e , whereas $G(\omega)$ signifies the Keldysh Green's function in presence of the full Hamiltonian \mathcal{H} . We are to take the lesser part of the product of the two Green's functions, which is realized by applying Langreth's rules [56]. The bare Green's functions of the electrons at the edge in the wide-band limit are given by

$$g_{\psi_\sigma \psi_\sigma^\dagger}^{r/a}(\omega) = \mp i \pi \rho_0, \quad (8)$$

$$g_{\psi_\sigma \psi_\sigma^\dagger}^<(\omega) = 2\pi \rho_0 f(\omega - \mu_\sigma),$$

with $g^{r(a)}$ the retarded (advanced) bare Green's function. We similarly label the fully dressed retarded (advanced) Green's function by $G^{r(a)}$. Using these functions and labels we express the backscattered current using only the fully dressed Green's functions of the d_σ orbitals

$$I_B = \frac{G_0}{e} \Gamma \int d\omega \left[G_{d_+}^<(\omega) + 2\Im\{G_{d_+}^r(\omega)\} f(\omega - \mu_+) \right. \quad (9)$$

$$\left. - G_{d_-}^<(\omega) - 2\Im\{G_{d_-}^r(\omega)\} f(\omega - \mu_-) \right].$$

Here, $\Gamma = \pi \rho_0 |t_\sigma|^2$ equals half the tunneling rate to the localized impurity orbital, which is identical for both σ due to time-reversal symmetry, and we used the shorthand notation $G_{d_\sigma}^\nu$ for the Green's functions $G_{d_\sigma d_\sigma^\dagger}^\nu$.

Eq. (9) is a central result of this section, as it is an exact expression for the non-equilibrium current through the edge $I = G_0 V - I_B$, driven by an applied voltage drop $eV = \mu_+ - \mu_-$. It can be evaluated by calculating the fully dressed Green's functions of the localized orbitals alone. No approximations were needed in its derivation from our Hamiltonian, and it encodes all the information about the correlations and temperature dependence

through the structure of the fully dressed Green's functions. Note, that the vanishing of the backscattered current is equivalent to $\langle \psi_\sigma^\dagger(0)d_\sigma \rangle = \langle d_\sigma^\dagger \psi_\sigma(0) \rangle$ implying that these expectation values are real. We now turn to a qualitative discussion, and point out the unique features of the helical edge.

The total current I is a current through a 1d mode which is *side-coupled* to an interacting region. Studies of transport in 1d channels side-coupled to an impurity in the Kondo regime have shown that such impurities suppress the conduction completely at low temperatures, in contrast to the perfect transmission when tunneling *through* Kondo correlated impurity [57]. However, the setups considered for these studies were markedly different than the setup described here, as both left and right movers carried both spin flavors, and respectively coupled to the Kondo impurity. In the helical edge setup, on the other hand, left and right movers correspond to different spin flavors. To illustrate the difference between these setups, which directly affects the current, we note that the helical edge Hamiltonian cannot be derived from a corresponding 1d lattice model when taking the continuum limit, and it is fundamentally different than the non-helical case. One has to bear in mind that the full model of the quantum spin-Hall insulator is 2d and the helical edge states are effective 1d topologically protected transport channels that can be spatially deformed. Therefore, the strong-coupling picture where side-coupling to an impurity cuts a 1d wire into two pieces, as the site near the impurity hybridizes strongly with it, is not applicable.

On the other hand, the backscattered current I_B describes a current contribution from source to drain *through* the impurity, and can be mapped onto a spinless model where two noninteracting leads are coupled through an interacting region. In this mapping the up-spin electrons in the edge are mapped onto a source lead, while the down-spin electrons are the drain. The requirement of time-reversal symmetry in the original Hamiltonian greatly restricts the type of terms allowed in the interacting region. Specifically, levels coupled to the source d_+ and levels coupled to the drain d_- cannot directly be linked as the term $\lambda d_+^\dagger d_-$ breaks time-reversal symmetry. In order to get non-vanishing backscattered current in steady state one must overcome this obstacle by considering additional interaction terms.

C. $U(1)$ symmetry and the current

In this section we define a $U(1)$ symmetry the system might maintain, and demonstrate its importance in protecting the perfect conductance of the edge even for finite bias and temperatures. We show that without explicitly breaking this symmetry no steady-state backscattered current can be driven by the local impurity. This is demonstrated by applying a time-dependent gauge transformations, and separately by employing Hershfield's Y -operator formalism.

While the $SU(2)$ symmetry is broken by the helical states, we can define a global $U(1)$ symmetry in absence of \mathcal{H}_D . The transformation $\psi_\sigma \rightarrow e^{i\sigma\theta} \psi_\sigma$, $d_\sigma \rightarrow e^{i\sigma\theta} d_\sigma$ leaves both \mathcal{H}_e and \mathcal{H}_t invariant and preserves time-reversal symmetry. This symmetry is equivalent to a global rotation about the joined spin z -axis of the electrons at the edge and the d_σ orbital. This can be further generalized to encompass degrees of freedom included only in \mathcal{H}_D . By summation, one can construct $\mathcal{S}^z = \mathcal{S}_{\text{mac}}^z + \mathcal{S}_{\text{mic}}^z$ with

$$\begin{aligned} \mathcal{S}_{\text{mac}}^z &= \sum_{\sigma} \sigma \int dx \psi_{\sigma}^{\dagger}(x) \psi_{\sigma}(x), \\ \mathcal{S}_{\text{mic}}^z &= \sum_{\sigma} \sigma \left[d_{\sigma}^{\dagger} d_{\sigma} + \sum_n D_{n,\sigma}^{\dagger} D_{n,\sigma}^o \right] + 2 \sum_j \mathcal{S}_j^z, \end{aligned} \quad (10)$$

where \mathbf{S}_j are the different possible spins degrees of freedom describing the impurity. Then the $U(1)$ rotation is generated by $\exp[i\theta \mathcal{S}^z/2]$. We have either $[\mathcal{S}^z, \mathcal{H}] = 0$ for the $U(1)$ symmetric case, or $[\mathcal{S}^z, \mathcal{H}] \neq 0$ when it is broken by \mathcal{H}_D .

We begin by applying a gauge transformation using the $U(1)$ generator of Eq. (10) $U_z(\tau) = \exp[-i\mathcal{S}^z(\mu_+ - \mu_-)\tau/2]$, transforming each of the operators according to their charge under \mathcal{S}^z . Following the transformation, an extra term is added to the Hamiltonian, given by

$$\Delta \mathcal{H} = i [\partial_{\tau} U_z(\tau)] U_z^{\dagger}(\tau),$$

which has a double effect. It shifts the energies of the left- and right-moving edge electrons and eliminates the chemical potential, and in addition, a local effective magnetic field is generated

$$\mathcal{H}_{B_{\text{eff}}} = \frac{\mu_+ - \mu_-}{2} \mathcal{S}_{\text{mic}}^z. \quad (11)$$

Operators and expectation values may acquire an explicit time-dependence, which reflects the fact that the setup is out of equilibrium.

In case the $U(1)$ symmetry is maintained, the Hamiltonian and the current operator remain time-independent after the transformation. Since the Hamiltonian and the current operator are time-independent, the problem is mapped onto an effective equilibrium problem, in presence of the local magnetic field, and all expectation values can be calculated with respect to the transformed Hamiltonian. In equilibrium, the fluctuation dissipation theorem ensures that $G^<(\omega) = -2\Im\{G^r(\omega)\}f(\omega)$ which renders the backscattered current in Eq. (9) identically zero at steady-state.

As \mathcal{S}^z is a conserved quantity in this case, and each backscattering event changes the values of $\mathcal{S}_{\text{mac}}^z$ by ± 2 , the values of the local $\mathcal{S}_{\text{mic}}^z$ must change accordingly by ∓ 2 with each backscattering event. Therefore, the coupling of the local degrees of freedom to the effective magnetic field ensures that each backscattering event costs or gains the correct amount of energy $\mu_{\sigma} - \mu_{-\sigma} = eV$. One can also use this fact to convince oneself that the

backscattered current must be zero at steady-state: Since S_{mic}^z is a local *microscopic* quantity, as long as S^z is a conserved quantity, S_{mic}^z can allow only a finite number of consecutive backscattering events in the same direction before reaching its maximal allowed value, blocking any further backscattering in that direction.

The situation is starkly different if the $U(1)$ symmetry is broken. In that case, while the current operator following the transformation is still time-independent, the Hamiltonian is bound to be explicitly dependent on time. The setup cannot be described any longer by an effective equilibrium Hamiltonian, and I_B may attain a non-zero value.

A different proof (but similar in spirit) can be constructed by employing the Y operator formalism developed by Hershfield [58] to describe non-equilibrium steady-state. In this formalism, the system is described in the distant past $t \rightarrow -\infty$ by the density matrix

$$\rho_0 = \frac{1}{Z_0} e^{-\beta(\mathcal{H}_0 - Y_0)} \quad (12)$$

with Y_0 the non-equilibrium condition, and then an interaction term \mathcal{H}_I is turned on adiabatically. The system evolves in time until steady-state is reached. The steady-state density matrix is given by a similar form,

$$\rho = \frac{1}{Z} e^{-\beta(\mathcal{H} - Y)} \quad (13)$$

with $Y = \sum_{n=0}^{\infty} Y_n$, where Y_n maintains

$$[\mathcal{H}_0, Y_n] - i\eta Y_n = [Y_{n-1}, \mathcal{H}_I] \quad (14)$$

for infinitesimal $\eta \rightarrow 0^+$.

Hershfield [58] decomposed the Y -operator into the general many-body scattering states operators $\Gamma_{k\sigma}$:

$$Y = \sum_{k\sigma} \mu_{k\sigma} \Gamma_{k\sigma}^\dagger \Gamma_{k\sigma} \quad (15)$$

where $\Gamma_{k\sigma}^\dagger$ is expanded in contributions $\Gamma_{k\sigma,n}^\dagger$ proportional to the interaction term $(\mathcal{H}_I)^n$ of the Hamiltonian

$$\Gamma_{k\sigma}^\dagger = \sum_{n=0}^{\infty} \Gamma_{k\sigma,n}^\dagger \quad (16)$$

and each component $\Gamma_{k\sigma,n}^\dagger$ ($n > 0$) obeys the hierarchical differential equation

$$\frac{d\Gamma_{k\sigma,n}^\dagger(t)}{dt} - i\epsilon_{k\sigma} \Gamma_{k\sigma,n}^\dagger = i[\Gamma_{k\sigma,n-1}^\dagger, \mathcal{H}_I]. \quad (17)$$

In order to shed some light into the nature of the Y -operator for the $U(1)$ symmetric case, we can evaluate the commutators in lowest order. Let us start with $\mathcal{H}_D = 0$, $\mathcal{H}_0 = \mathcal{H}_e$ and treat the bilinear term \mathcal{H}_t as interaction. The equations can be analytically solved yielding the single-particle Lippmann-Schwinger states operators stated below in Eq. (20) ($\Gamma_{k\sigma}^\dagger = \gamma_{k,\sigma}^\dagger$). The term $\Gamma_{k\sigma}^\dagger \Gamma_{k\sigma}$

counts the number of fermions in the system with a spin σ projection, hence

$$Y = \frac{\mu_+ - \mu_-}{2} S^z - \frac{\mu_+ + \mu_-}{2} \hat{N}_{\text{tot}} \quad (18)$$

where \hat{N}_{tot} counts the total number of fermions in the system, and the scattering states operators $\gamma_{k,\sigma}^\dagger$ can be used to write the Hamiltonian $\mathcal{H}_e + \mathcal{H}_t$ in energy diagonal form.

Now we add a finite \mathcal{H}_D that is conserving the total spin component S^z , typically an anisotropic Heisenberg term. The number of left- and right-movers are no longer individually conserved, and these states mix due to the interaction in Eq. (17). However, each mixing term is always associated with a local spin-flip operator S^\pm , so that the contribution $\Gamma_{k\sigma,n}^\dagger$ maintains its spin excitation character in all orders of the hierarchy so that $\Gamma_{k\sigma}^\dagger$ remains an eigenoperator of the total spin component S^z . Now $\Gamma_{k\sigma}^\dagger \Gamma_{k\sigma}$ counts the number of spin σ excitations in the system and Eq. (18) remains valid even for $\mathcal{H}_D \neq 0$ as long as $[\mathcal{H}, S^z] = 0$. Note, that one can either construct $\gamma_{k,\sigma}^\dagger$ for $\mathcal{H}_D = 0$ and then perform a second step by setting $\Gamma_{k\sigma,0}^\dagger = \gamma_{k,\sigma}^\dagger$ and switch on $\mathcal{H}_D = 0$, or one starts directly from free edge states and use $\mathcal{H}_I = \mathcal{H}_t + \mathcal{H}_D$ to arrive at the same final $\Gamma_{k\sigma}^\dagger$.

The density operator is equivalent to the equilibrium operator in a finite magnetic field since the first term in Y corresponds to a global magnetic field applied in z -direction. The second term control the overall filling with fermions and can be essentially dropped. Note that while the occupation numbers are governed by $\rho \propto \exp[-\beta(\mathcal{H} - Y)]$, the dynamics is only controlled by the Hamiltonian \mathcal{H} itself. This is important for calculating the Green's functions. One can either carry out an equilibrium calculation with respect to $\mathcal{H}' = \mathcal{H} - Y$ and perform a frequency shift by $\mu_{k\sigma}$ by hand at the end, or use the definition of the Heisenberg operator $O(t) = \exp[i\mathcal{H}t]O \exp[-i\mathcal{H}t]$ to obtain the correct frequency spectrum. We adopted the later scheme since it remains valid in true non-equilibrium situations when the $U(1)$ symmetry is broken.

In the pseudo-equilibrium situation where the $U(1)$ symmetry holds, the spectral functions obey the dissipation-fluctuation theorem and, therefore, the backscattering current I_B vanishes identically. Although the operators $\Gamma_{k\sigma}^\dagger$ contain mixing of left- and right-movers, the mixing cannot induct a steady-state backscattering current. This can be understood in a consecutive application of $\Gamma_{k\sigma}^\dagger$ onto some arbitrary many-body quantum state. Since each backscattering term is associated with a local spin-flip term, and the local spin has a finite length, these backscattering terms do not contribute in higher order since they lead to a nil state or to an equal number of back and forth scattering such that the net current always vanished. This is fundamentally different of a $U(1)$ symmetry breaking interaction.

In conclusion, we showed breaking the $U(1)$ symmetry

defined by \mathcal{S}^z of Eq. (10) is critical in order for the local impurity to drive a backscattering current at steady-state. When $[\mathcal{S}^z, \mathcal{H}] = 0$, the system can always be mapped onto an effective equilibrium setup, which leads to a vanishing backscattering current [given in Eq. (9)] due to the fluctuation-dissipation theorem. Following this mapping, the non-equilibrium condition plays a role of a magnetic field. Therefore, we must introduce into \mathcal{H}_D terms that do not commute with \mathcal{S}^z in order to obtain finite backscattering current.

III. INTERACTION HAMILTONIAN AND PERTURBATIVE RG ANALYSIS

From now on forward we shall consider a specific form of interaction for \mathcal{H}_D . If one considers a localized impurity spin-1/2 which interacts with a single spinfull d -level, then the most general interaction Hamiltonian that respects time-reversal symmetry is given by

$$\begin{aligned} \mathcal{H}_D = & \epsilon_d \sum_{\sigma=\pm} \hat{n}_\sigma + U \hat{n}_+ \hat{n}_- \\ & + \sum_{\alpha, \beta, \nu, \nu'} J_{\alpha, \beta} S^\alpha d_\nu^\dagger \sigma_{\nu, \nu'}^\beta d_{\nu'}. \end{aligned} \quad (19)$$

Here, $\hat{n}_\sigma = d_\sigma^\dagger d_\sigma$, $\sigma_{\nu, \nu'}^\beta$ are matrix elements of the Pauli matrices and $J_{\alpha, \beta}$ is a set of nine real coupling coefficients. We used the indices ν, ν' in this sum for the helical label σ in order to distinguish the label from the symbol for the Pauli matrices. The first two terms describe the on-site energy and Coulomb repulsion between the levels, while the last term is a time-reversal symmetric exchange coupling between the spinfull d -level and the impurity spin. We note that when considering the case of an impurity spin with spin larger than 1/2, the Hamiltonian may also include spin-anisotropy terms $M_\alpha (S^\alpha)^2$ which are nontrivial. These terms may play an important role in driving backscattering current in such setups [48, 50].

A. Mapping onto the anisotropic Kondo Hamiltonian

It is instructive to map the Hamiltonian onto the well-studied Kondo Hamiltonian. To this end, we start by diagonalizing $\mathcal{H}_e + \mathcal{H}_t$ exactly using the helical scattering states, given by

$$\begin{aligned} \gamma_{k, \sigma}^\dagger = & e^{i\phi_k} \psi_{k, \sigma}^\dagger + \frac{t_\sigma}{\sqrt{2\pi}} |g_{d_\sigma}(\epsilon_k + i\eta)| \\ & \times \left(d_\sigma^\dagger + \int \frac{dk'}{\sqrt{2\pi}} \frac{t_\sigma}{\epsilon_k - \epsilon_{k'} + i\eta} \psi_{k', \sigma}^\dagger \right), \end{aligned} \quad (20)$$

that can be derived from Eq. (17) [59]. Here,

$$g_{d_\sigma}(z) = \left[z - \int \frac{dk}{2\pi} \frac{|t_\sigma|^2}{z - \epsilon_k} \right]^{-1}$$

is the Green's function associated with the level d_σ , and $\phi_k = \arg\{g_{d_\sigma}(\epsilon_k - i\eta)\}$ its phase. The eigenmodes maintain the canonical fermionic anti-commutation relations and are characterized by definite charge and spin/helicity σ .

The non-interacting Hamiltonian is expressed in its eigenmodes $\gamma_{k, \sigma}$

$$H_e + \mathcal{H}_t = \sum_\sigma \int dk \epsilon_k \gamma_{k, \sigma}^\dagger \gamma_{k, \sigma}. \quad (21)$$

They also allow us to write the localized level operators as

$$d_\sigma = \int \frac{dk}{\sqrt{2\pi}} t_\sigma |g_{d_\sigma}(\epsilon_k + i\eta)| \gamma_{k, \sigma}. \quad (22)$$

The interacting Hamiltonian is then given by

$$\begin{aligned} \mathcal{H}_D = & \epsilon_d \sum_\sigma t_\sigma^2 \int \frac{dkdk'}{2\pi} |g_{d_\sigma}(\epsilon_k + i\eta)| |g_{d_\sigma}(\epsilon_{k'} - i\eta)| \gamma_{\sigma, k'}^\dagger \gamma_{k, \sigma} \\ & + U t_+^2 t_-^2 \int \frac{dkdk' dqdq'}{(2\pi)^2} |g_{d_+}(\epsilon_k + i\eta)|^2 |g_{d_-}(\epsilon_{k'} + i\eta)|^2 \gamma_{k, +}^\dagger \gamma_{k', +} \gamma_{q', -}^\dagger \gamma_{q, -} \\ & + \sum_{\alpha, \beta, \nu, \nu'} J_{\alpha, \beta} S^\alpha t_\nu t_{\nu'} \int \frac{dkdk'}{2\pi} |g_{d_\nu}(\epsilon_k + i\eta)| |g_{d_{\nu'}}(\epsilon_{k'} - i\eta)| \gamma_{k', \nu'}^\dagger \sigma_{\nu', \nu}^\beta \gamma_{k, \nu}, \end{aligned} \quad (23)$$

where we again used ν, ν' instead of σ, σ' in the last term in order to avoid confusion with the notation for the Pauli matrices. Due to the time-reversal symmetry, $t_+ = t_- \equiv t$ and $g_{d_\nu}(\omega \pm i\eta) = (\omega \pm i\Gamma)^{-1}$ where $\Gamma = \pi\rho_0 t^2$. Note that for this derivation we assumed a wide band limit,

$D \gg \Gamma, \omega, eV$, so that the real part of the self-energy of g_{d_ν} can be neglected.

In the limit where $U = 0 = \epsilon_d$, this Hamiltonian is an anisotropic spin-1/2 Kondo Hamiltonian. To see this, we observe that the J term is an exchange coupling between

the local spin-density of the γ_{\pm} quasiparticles and the local impurity spin $\mathcal{H}_J = \sum_{\alpha,\beta} J_{\alpha,\beta} S^{\alpha} \sigma^{\beta}(0)$ where

$$\sigma(0) = \sum_{\nu,\nu'} \int dk dk' \sqrt{\rho_{\gamma}(k) \rho_{\gamma}(k')} \gamma_{\nu,k}^{\dagger} \sigma_{\nu,\nu'} \gamma_{\nu',k'}. \quad (24)$$

Here $\pi \rho_{\gamma}(k) = \Gamma |g_d(\epsilon_k)|^2$ is an effective density of states of the γ_{\pm} modes that couple to the spin, and Γ serves as the bandwidth. In this limit, the setup is characterized by a single Kondo scale T_K for an antiferromagnetic coupling tensor $J_{\alpha,\beta}$. At temperatures below that scale $T \ll T_K$, the local impurity spin will be screened by the γ -quasiparticles, and the local magnetic moment asymptotically vanish for $T \rightarrow 0$ as a Kondo singlet is formed.

As we are mainly interested in the role of the exchange anisotropy on the backscattered current, we will focus first and foremost on the limit where both $U = 0$ and $\epsilon_d = 0$. We qualitatively discuss how turning them on affects the physics of the setup in subsection III D.

B. One-loop RG equations and flow

The advantage of mapping \mathcal{H} onto the Kondo Hamiltonian is the exploitation of the rich nomenclature and the extensive knowledge of this model. Specifically, the perturbative renormalization group analysis of the Hamiltonian provides already a significant insight into the properties of the setup.

The exchange couplings $J_{\alpha,\beta}$ constitute a tensor, where the first index signifies a component of a vector in the spin space of the quasiparticles $\gamma_{k,\sigma}$ while the second index is a part of a vector in the spin space of the impurity spin. For this section, it will be convenient to write this tensor as comprised of three vectors in the spin-impurity space $\mathbf{J}_{\beta=x,y,z}$. Each of this vectors is $\mathbf{J}_{\beta} = \sum_{\alpha} J_{\alpha,\beta} \hat{x}_{\alpha}$ with \hat{x}_{α} being a unit vector in the α direction of the impurity spin. In this notation, \mathbf{J}_{β} couples to the β component of the quasiparticles spin density $\sigma^{\beta}(0)$.

We carry out a poor man's scaling calculation on this setup, in the weak-coupling limit where $|\mathbf{J}_{\alpha}| \ll \Gamma$. We relegate the details of the calculations to Appendix A and present and discuss here its results. The RG flow equations close to the local moment fixed point are given by the general expression

$$\frac{d\mathbf{J}_{\alpha}}{d\lambda} = \pi^2 \rho_0 \epsilon_{\alpha\beta\gamma} \mathbf{J}_{\beta} \times \mathbf{J}_{\gamma}, \quad (25)$$

where $\lambda = \ln(D/D')$ is the logarithm of the running cutoff D' .

A detailed analysis of these equations can be found in the appendix of Ref. [60]. We only present and discuss its main finding here. There are six conserved quantities under this set of equations $a_{\alpha,\beta} = \mathbf{J}_{\alpha} \cdot \mathbf{J}_{\beta} = |\mathbf{J}_{\alpha}| |\mathbf{J}_{\beta}| \cos(\theta_{\alpha,\beta})$ and $b_{\alpha,\beta} = |\mathbf{J}_{\alpha}|^2 - |\mathbf{J}_{\beta}|^2$ for $\alpha \neq \beta$.

For the convenience of the discussion, let us focus now on $a_{x,y}$ and $b_{x,y}$. If $a_{x,y} = 0$ and $b_{x,y} = 0$ then the coupling is isotropic with $\mathbf{J}_x \perp \mathbf{J}_y$ and $|\mathbf{J}_x| = |\mathbf{J}_y|$,

and the $U(1)$ symmetry is maintained. On the other hand, if $a_{x,y}$ and $b_{x,y}$ are nonzero, then $U(1)$ symmetry is broken. However, at the strong coupling fixed point $|\mathbf{J}_x|, |\mathbf{J}_y| \rightarrow \infty$, from which we can derive

$$\begin{aligned} \frac{\mathbf{J}_x \cdot \mathbf{J}_y}{|\mathbf{J}_x| |\mathbf{J}_y|} &= \frac{a_{x,y}}{|\mathbf{J}_x| |\mathbf{J}_y|} \rightarrow 0, \\ \frac{|\mathbf{J}_x|^2 - |\mathbf{J}_y|^2}{|\mathbf{J}_x|^2 + |\mathbf{J}_y|^2} &= \frac{b_{x,y}}{|\mathbf{J}_x|^2 + |\mathbf{J}_y|^2} \rightarrow 0. \end{aligned} \quad (26)$$

The implication of these limits is that as the magnitude of $|\mathbf{J}_x|$ and $|\mathbf{J}_y|$ increase during the RG flow, they flow toward being perpendicular and similar in magnitude. This process describes a dynamical restoration of the $U(1)$ symmetry, and the strong coupling fixed point is isotropic.

We note that not all initial couplings will flow to the strong coupling fixed point, as it is well known that the ferromagnetic Kondo model, with $\mathbf{J}_x = J_{\perp} \hat{x}$, $\mathbf{J}_y = J_{\perp} \hat{y}$ and $\mathbf{J}_z = J_z \hat{z}$ where $J_z < -|J_{\perp}| < 0$, flows to a fixed point where $\mathbf{J}_{x,y} \rightarrow 0$. In this case as well, $a_{x,y}$ and $b_{x,y}$ are zero throughout the entire RG flow, and $U(1)$ symmetry is maintained.

As shown in Ref. [60], the backscattering rate is related to the anisotropy and measured by the scale

$$J_B = \left[\frac{(|\mathbf{J}_x|^2 - |\mathbf{J}_y|^2)^2 + 4(\mathbf{J}_x \cdot \mathbf{J}_y)^2}{J_x^2 + J_y^2} \right]^{1/2}. \quad (27)$$

Note that the \mathbf{J}_z term cannot contribute to the backscattering, since it cannot break the $U(1)$ symmetry. Furthermore, if $\mathbf{J}_x \perp \mathbf{J}_y$ and both vectors are of the same length, $J_B = 0$. This defines the line of $U(1)$ symmetric points on which the backscattering current vanishes. The numerator of J_B is constant under the perturbative RG flow, as it is composed of the conserved $a_{x,y}$ and $b_{x,y}$, while the denominator increases under the flow toward the strong-coupling fixed point. As the low-energy strong-coupling fixed point is isotropic and restores the $U(1)$ symmetry dynamically, we expect the backscattering to vanish when the system reaches that strong coupling fixed point that is beyond the scope of the perturbative RG analysis.

The formation of the Kondo singlet characterized by the $U(1)$ symmetry is associated with an energy scale T_K . In the low-temperature and small bias voltage limit $|eV|, T \ll T_K$, the perfect conductance of the edge will be restored as the backscattering current asymptotically vanishes for $T \rightarrow 0$ and $eV \rightarrow 0$. As either the temperature or the bias voltage increases above T_K , the RG flow is stopped before the singlet is formed, and the backscattering current may retain a finite value for an initially $U(1)$ symmetry breaking \mathcal{H}_D .

C. Exactly solvable point

If only one component of the exchange coupling \mathbf{J}_{α} is nonzero, the interacting problem can be solved exactly.

In this case, the projection of \mathbf{S} parallel to \mathbf{J}_α is a good quantum number and can be diagonalized together with the Hamiltonian. One implication of only one of \mathbf{J}_α being nonzero is the absence of any RG flow $d\mathbf{J}_\alpha/d\lambda = 0$.

As we are interested in exchange coupling that breaks the $U(1)$ symmetry we discuss here the setup where only the component J_{xx} is nonzero. As S^x is a good quantum

number, we can diagonalize the Hamiltonian separately for $S^x = \pm 1$. In each sector, the interaction term generates backscattering, where the two sectors are related by time-reversal symmetry.

The fully dressed Green's functions matrices for the d orbitals are given by

$$\mathcal{G}_d^{r/a}(\omega) = \frac{1}{(\omega \pm i\Gamma)^2 - J_{xx}^2} \begin{bmatrix} \omega \pm i\Gamma & J_{xx}S^x \\ J_{xx}S^x & \omega \pm i\Gamma \end{bmatrix},$$

$$\mathcal{G}_d^<(\omega) = \frac{2\Gamma}{|(\omega \pm i\Gamma)^2 - J_{xx}^2|} \begin{bmatrix} (\omega^2 + \Gamma^2)f_+ + J_{xx}^2f_- & J_{xx}S^x(\omega + i\Gamma)f_+ + J_{xx}S^x(\omega - i\Gamma)f_- \\ J_{xx}S^x(\omega - i\Gamma)f_+ + J_{xx}S^x(\omega + i\Gamma)f_- & (\omega^2 + \Gamma^2)f_- + J_{xx}^2f_+ \end{bmatrix}, \quad (28)$$

with the shorthand $f_\pm = f(\omega - \mu_\pm)$.

Plugging these expressions into the formula for the current of Eq. (9) and adding the contribution I_0 as stated in Eq. (5), the full current reads

$$I(eV) = G_0V - 4\frac{G_0}{e}J_{xx}^2\Gamma^2 \int \frac{(f_+ - f_-)d\omega}{|(\omega + i\Gamma)^2 - J_{xx}^2|^2}. \quad (29)$$

At zero temperature the differential conductance approaches

$$\frac{1}{G_0} \frac{dI}{dV} = 1 - \left[\frac{2J_{xx}^2\Gamma^2}{|(\frac{eV}{2} - i\Gamma)^2 - J_{xx}^2|^2} + \frac{2J_{xx}^2\Gamma^2}{|(\frac{eV}{2} + i\Gamma)^2 - J_{xx}^2|^2} \right]. \quad (30)$$

We note that this is a time-reversal symmetric setup of the Hamiltonian, where even at zero temperature the zero-bias conductance is not unity and decreases to zero at the point where $|J_{xx}| = \Gamma$. This further illustrates our claim that it is the $U(1)$ symmetry, and not the time-reversal symmetry, that protects the perfect conductance.

D. Nonzero ϵ_d and U

In this section we discuss qualitatively how the previous results are altered when ϵ_d and U are turned on. The two terms have a significantly different effect. The ϵ_d term does not affect the results substantially, as it adds a local potential scattering which is marginal in the RG flow, and as long as $\epsilon_d \ll D$, D being the bandwidth, the Kondo singlet will still form as before. At the exactly solvable point discussed above, the addition of ϵ_d (for $U = 0$) is directly incorporated into the Green's functions and the result in that limit is

$$I(eV) = G_0V - 4\frac{G_0}{e}J_{xx}^2\Gamma^2 \int \frac{(f_+ - f_-)d\omega}{|(\omega - \epsilon_d + i\Gamma)^2 - J_{xx}^2|^2}. \quad (31)$$

On the other hand, a finite U requires a more delicate discussion. We will separate it into two distinct cases: one without exchange interactions $J_{\alpha,\beta} = 0$ and one where the coupling to the impurity spin is turned on.

1. The $J_{\alpha,\beta} = 0$, $U \neq 0$ case

Let us first consider the case where the exchange coupling is turned off $J_{\alpha,\beta} = 0$ but with finite positive $U > 0$. The right and left movers have no way to exchange particles, and $\hat{N}_\pm + d_\pm^\dagger d_\pm$ are conserved quantities. The backscattered current is therefore zero regardless of the non-equilibrium conditions. Nevertheless, the physics of this setup are worth discussing.

This is the single impurity Anderson model (SIAM), and for $U > 0$ we know that a Kondo peak is created in the density of states of the d -orbitals below the Kondo temperature T_K^d and at zero bias if the local orbital occupancy is maintained near integer valence of one: the localized level form a singlet with the conductance electrons. Note that this scale T_K^d differs from the Kondo scale generated by a finite $J_{\alpha,\beta}$.

At finite bias the system is equivalent to a system in equilibrium with a local magnetic field applied to the localized levels as pointed out in Sec. II C. Note that this is a very subtle point: \mathcal{H} has complex strongly-correlated many-body eigenstates and the many-body scattering states $\Gamma_{k\sigma}$ contain mixtures of right-moving and left-moving edge states. However, the conservation of left and right movers prevents mixing of spin excitations and the non-equilibrium Y operator maintains the form of a Zeeman term, as $[\mathcal{S}^z, \mathcal{H}] = 0$ still holds. Time reversal symmetry is maintained by the Hamiltonian and only broken by the externally applied bias that enters in the Y operator and drives the edge current I .

2. Finite U and weak $J_{\alpha,\beta}$

We also briefly consider the case where both $U > 0$ and $J_{\alpha,\beta}$ are finite. Starting from $J_{\alpha,\beta} = 0$ and $\epsilon_d + U > 0$, the Hamiltonian approaches the strong coupling fixed point [53] below T_K^d . This fixed point describes a local Fermi liquid that can be treated as a free electron gas for $|\omega| < T_K^d$ in leading order. Switching on an antiferromagnetic $J_{\alpha,\beta}$ leads to another Kondo effect [59] involving the screening of the local spin below the temperature T_K^s that is exponentially dependent on the $J_{\alpha,\beta}$ [61]. This picture remains valid for $T_K^s \ll T_K^d$ and generates a pseudo-gap in the full renormalized orbital spectral function $\rho_d(\omega)$.

We derive an expression for the backscattered current by treating J perturbatively and then follow a similar approach to the one taken above for the exactly solvable point. Since a $U(1)$ symmetric $J_{\alpha,\beta}$ leads to vanishing I_B we restrict ourselves to a finite J_{xx} term and set all other $J_{\alpha,\beta} = 0$. In leading order in J_{xx} , backscattering happens between the two local Fermi liquids. The backscattered current will therefore be

$$I_B \sim \frac{G_0}{e} J_{xx}^2 \int \rho_+(\omega) \rho_-(\omega) (f_+ - f_-) d\omega, \quad (32)$$

where $\rho_{\pm}(\omega)$ is the renormalized density of states of d_{\pm} , including the effects of t, ϵ_d as well as U . We wrote J_{xx} for connection with the formula in Eq. (31), but one has to sum over all terms $J_{\alpha,\beta}$ that allow backscattering.

Let's assume we have finite U and J and two Kondo scales T_K^d and T_K^s . If J is large then the local spin and the d orbital will form a singlet and decouple from the edge. For small J , the argumentation above holds and the d orbital will get screened at first and then screen the local spin in turn. This leaves us with two distinctly different GS for small and large J . The parameter space of weak and strong $J_{\alpha,\beta}$ and a finite U are adiabatically connected: Since there is no quantum phase transition in the parameter space we leave the analysis of the full parameter space where both $J_{\alpha,\beta}$ and U are finite and comparable to a later study. Here, we are interested on the fundamental mechanism generating a backscattered current I_B in a time-reversal symmetric Hamiltonian. From now on we mostly discuss the case where $U = 0$, which will allow us to focus on the role of the exchange coupling anisotropy. In this case, the Kondo temperature T_K^d is maximal and replaced by Γ . Therefore we always choose the parameters for the numerical simulation such that $T_K^s < \Gamma$.

IV. NUMERICAL ANALYSIS

A. Time-Dependent Numerical Renormalization Group and Green's Functions

The backscattering current Eq. (9) requires calculation of the non-equilibrium retarded and lesser Green's func-

tions. Since we are interested in the low-temperature behavior for arbitrary interaction strength $J_{\alpha,\beta}$ as well as a wide range of bias voltages, we opt for the TD-NRG [62, 63], which has been used successfully to calculate steady-state Green's Functions in the context of transport through single-orbital quantum dots before [64, 65]. It also allows to access the low-energy fixed point in equilibrium of the model introduced in Sec. III and, therefore, test the predictions of the analytical perturbative RG approach outlined above.

The NRG was originally developed by Wilson [61] to solve the single-channel Kondo problem but has been extended to various problems describing magnetic impurities coupled to a host's conduction bands in the meantime. The general Hamiltonian, as discussed in Sec. II, can be partitioned into three parts

$$\mathcal{H} = \mathcal{H}_D + \mathcal{H}_e + \mathcal{H}_t, \quad (33)$$

where \mathcal{H}_D and \mathcal{H}_e contains impurity or edge degrees of freedom only. The impurity part may comprise local many-body interactions of arbitrary strength. The edge states, however, are taken to be non-interacting and play the role of the quasi-continuous band in the conventional NRG. The third term \mathcal{H}_t describes a hybridization between the localized impurity and the edge states. In the NRG scheme, one proceeds by partitioning the hybridization function $\Gamma(\omega)$ into logarithmically shrinking intervals around the chemical potential with help of the dimensionless discretization parameter $\Lambda > 1$. The edge degrees of freedom are rewritten as linear combinations of operators for each such interval. Only modes that couple directly to the impurity are retained at this point. The system is further transformed by a tridiagonalization algorithm and mapped onto a semi-infinite tight-binding chain, the so-called Wilson chain, where the first chain link is equivalent to \mathcal{H}_D . The system is now solved in an iterative fashion where one diagonalizes the Hamiltonian for a given chain length, calculates expectation values of interest, and proceeds by adding the next chain link. The tight-binding hopping parameters of such a chain fall off exponentially as one traverses the chain which is a direct result of the logarithmic discretization of the hybridization function. Due to the exponentially decreasing hopping elements, the Hamiltonian of a given iteration can be linked to a likewise decreasing temperature scale [53, 61]. The iterative scheme is terminated at some finite chain length N that determines the target temperature $T_N \sim \Lambda^{-N/2}$.

Only the N_s states with the smallest eigenvalues are kept each iteration and coupled to the next chain link in order to tackle the otherwise exponentially growing Fockspace. Furthermore, we employ Oliveira's z averaging [66] to suppress discretization artifacts and improve numerical precision.

In the TD-NRG [62, 63], we regard the system to be in thermal equilibrium for $t < 0$, at which point an additional interaction term $\Delta\mathcal{H}$ is turned on. Thus, the

Hamiltonian undergoes an abrupt change (or quench)

$$\mathcal{H}^i \rightarrow \mathcal{H}^f(t > 0) = \mathcal{H}^i + \Delta\mathcal{H}. \quad (34)$$

As a result, the density operator for $t > 0$ evolves in time with respect to the final Hamiltonian \mathcal{H}^f

$$\rho(t > 0) = e^{-i\mathcal{H}^f t} \rho_0 e^{i\mathcal{H}^f t}. \quad (35)$$

The equilibrium NRG scheme described above needs a further refinement since non-equilibrium calculations involve contributions from all energy scales intermingled together. One can show [62, 63] that a set of all discarded states form a complete basis for a Wilson chain of length N . Conceptually, one first carries out two separate equilibrium NRG calculations for \mathcal{H}^i and \mathcal{H}^f respectively. The eigenbasis of the final Hamiltonian is needed for the time-evolution of any operator $O(t)$ while the reduced density matrix is constructed in the eigenbasis of the initial Hamiltonian. The overlap matrix S_m allows for rotation between both bases at given iteration m and connects both NRG runs.

The approach outlined above can be straightforwardly extended for equilibrium spectral functions in their Lehmann representation [67, 68]. The TD-NRG and the sum-rule conserving scheme for the spectral functions were combined in Ref. [69] to evaluate non-equilibrium Green's functions for times t, t' . Note that both, the equilibrium and the non-equilibrium calculations, can be extended readily to lesser and greater Green's functions [68, 69]. The spectral δ -functions of the Lehmann representation are broadened by a logarithmic Gaussian as defined in Eq. (74) in Ref. [53], where we used the broadening parameter $b = 0.8$ throughout the paper.

Evaluation of the backscattering current Eq. (9) poses a number of challenges from a technical point of view. First, the calculations of the non-equilibrium Green's functions themselves according to the TD-NRG procedure. Second, we are not able to employ the improvement of the NRG Green's function via an equation of motion [70] since it is not readily applicable for non-equilibrium lesser Green's functions. Third, we need to calculate a difference between retarded spectral function and lesser Green's function, that may well be very small, before integrating numerically over the whole real axis. Finally, we are interested in the linear conductance $G = I_B/V$ which limits our precision further and keeps us effectively from using arbitrary small bias voltages since the already small current I_B cannot be distinguished from numerical noise in the limit $V \rightarrow 0$.

In the following we choose a discretization parameter $\Lambda = 2$, a half-bandwidth $D/\Gamma = 100$, and z averaging of $z = 4$ for all our calculations. If not stated otherwise, we use a Wilson chain of length $N = 45$ which results in a target temperature $T/\Gamma \approx 1.79 \cdot 10^{-5}$. This choice of parameters guarantees that the temperature T for our calculations is well below the equilibrium Kondo temperature T_K^{eq} as we will discuss in the next section.

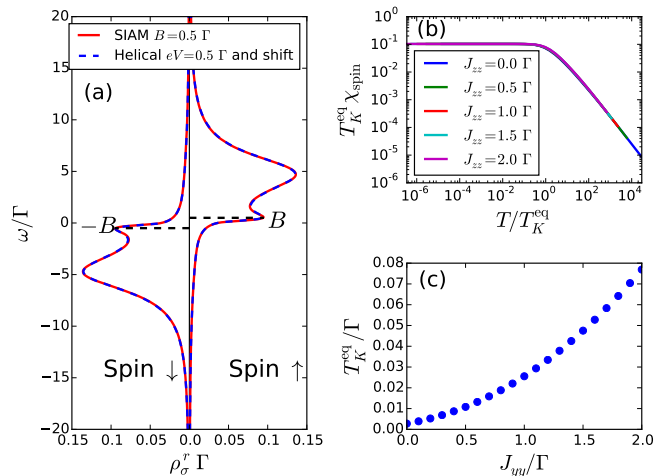


FIG. 2. (a) $\rho_\sigma^{r,\text{SIAM}}$ (red solid line) for finite magnetic field $B/\Gamma = 0.5$ compared to $\rho_\sigma^{r,\text{helical}}$ (blue dashed line) calculated for bias voltage $eV/\Gamma = 0.5$ and $J_{\alpha\beta} = 0$. The results for the helical model are shifted by an additional $\pm eV/2$. For both models $\epsilon_d/\Gamma = -5$ and $U/\Gamma = 10$. (b) Local spin susceptibility χ_{spin} for helical model in equilibrium $eV = 0$, $\epsilon_d/\Gamma = -0.5$, $U = 0$, and $J_{xx} = J_{yy} = \Gamma$. (c) Equilibrium Kondo temperature calculated from the local spin susceptibility as a function of J_{yy} for $J_{xx} = J_{zz} = \Gamma$ and $U = \epsilon_d = 0$.

B. Equilibrium and effective equilibrium

We start by addressing the setup in equilibrium. While we are mostly interested in the case where $U = 0$ and $J_{\alpha,\beta} \neq 0$, it is instructive to first consider the opposite case where U is finite and $J_{\alpha,\beta}$ are turned off. Under this conditions, the additional spin completely decouples from the subsystem comprising the local d orbital and the edges, and the system is equivalent to an equilibrium Single Impurity Anderson Model (SIAM).

We performed two independent NRG calculations: a conventional equilibrium NRG calculation of a SIAM in a finite magnetic field, and a full scattering states TD-NRG calculations where the bias enters through the Y operator in the density operator but the dynamics is governed by the Hamiltonian only [69]. Remarkably, as discussed above, the system remains in effective equilibrium even when a finite bias voltage is applied, as the two spin-flavors are only capacitively connected. When a bias voltage eV is applied, the system behaves as under the influence of a magnetic field B where the chemical potential difference takes on the role of the Zeeman energy. Here, the Kondo peak resides at $\pm B$ for spin up and spin down, thus accounting for a splitting of $\Delta E = g_{\text{eff}} B$ while the Kondo peak forms around the respective chemical potential in the helical model. As a result, the spectral density of the equilibrium SIAM calculation $\rho_\sigma^{r,\text{SIAM}}$ shows a peak at double the chemical potential of the opposite spin on an absolute scale [Fig. 2 (a)]. Perfect agreement can be realized by a symmetric shift of $\pm eV/2$.

We are ultimately interested in the backscattered current driven by finite exchange coupling to the local spin. In order to examine the role of the anisotropy, we turn on a finite $J_{\alpha,\beta}$ and set $U = 0$. The finite U regime is adiabatically connected but results in a much lower characteristic energy scale. In equilibrium $eV = 0$, this setup is also characterized by a Kondo screening, which is different than the Kondo screening for the SIAM setup (finite U and zero exchange coupling) discussed before. The Kondo temperature associated with this exchange coupling can be found numerically by employing Wilson's definition using the temperature dependent magnetic susceptibility via $4T_K^{\text{eq}}\chi_{\text{spin}}(T_K^{\text{eq}}) = 0.413$ [53, 61]. Here, $\chi_{\text{spin}}(T)$ is calculated by applying an infinitesimal small local magnetic field and measuring the polarization of the localized spin (not the spin of the d electron) in absence of a bias voltage $eV = 0$ [Fig. 2 (b)]. In the following, we will refer to the equilibrium Kondo temperature calculated in this way as T_K^{eq} to emphasize that it stems from an equilibrium calculation. To simplify the discussion, we restrict ourselves to exchange couplings that contain only diagonal terms $J_{\alpha,\alpha}$. We note that it is sufficient to tune the ratio J_{xx}/J_{yy} to break $U(1)$ symmetry and generate a backscattered current, as discussed above (Sec. II C). This has the added benefit of eliminating complex terms from the local Hamiltonian, simplifying the numerical calculations. We also take advantage of the fact that J_{zz} does not affect the $U(1)$ symmetry, and we can set it at will. For the $U(1)$ symmetric point where $J_{xx} = J_{yy} = J_{zz} = \Gamma$, we get an equilibrium Kondo temperature $T_K^{\text{eq}}/\Gamma \approx 0.025$ [Fig. 2 (c)].

C. Finite backscattered current for $eV > T_K^{\text{eq}} \gg T$

We start at the symmetrical point $J_{xx} = J_{yy} = \Gamma$ and turn on a gate voltage eV on the edge. Below, we quantify the deviation from the $U(1)$ symmetric point by $\Delta J_{yy} = J_{yy} - \Gamma$ and retain the other two exchange parameter at fixed values $J_{xx} = J_{zz} = \Gamma$. The problem thus becomes a full non-equilibrium one. Both the lesser Green's function (GF) $G_{\sigma}^{<}$ and the spectral function ρ_{σ}^r times Fermi function fall off at the chemical potential for the respective spin σ . In the symmetrical case, the system can be mapped to an effective equilibrium problem and the lesser GF is equal to the retarded spectral function times the Fermi function and appropriate constant factor as a direct consequence of the fluctuation-dissipation theorem [Fig. 3 (a) and (b)]. We break the $U(1)$ symmetry by performing a quench in the value of ΔJ_{yy} . In the asymmetrical case and for $eV > T_K^{\text{eq}}$, the non-equilibrium lesser GF and retarded spectral density start to differ [Fig. 3 (c) and (d)] which consequently drives a backscattering current. The NRG GF broadening induces small finite size oscillations [53] in the spectral functions at the chemical potentials and the numerical integration. This effectively limits our precision for the backscattered conductance calculated by the integral over the difference

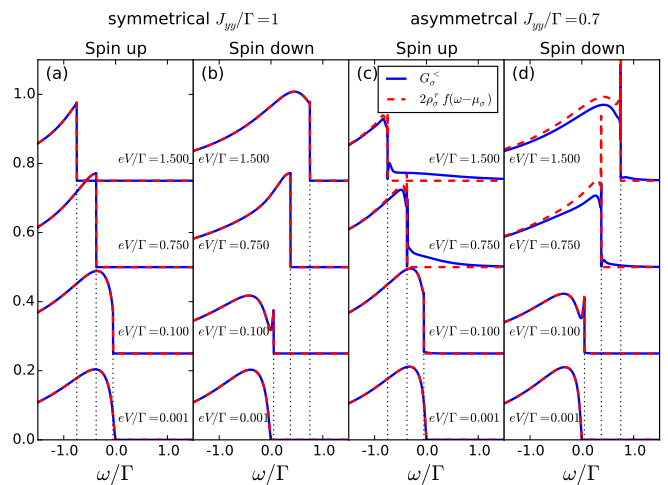


FIG. 3. $G_{\sigma}^{<}(\omega)$ (solid blue curves) and $2\rho_{\sigma}^r(\omega)f(\omega - \mu_{\sigma})$ (dashed green curves) for (i) the symmetrical point $J_{yy}/\Gamma = 1$ for spin (a) up and (b) down and (ii) for the broken $U(1)$ symmetry, $J_{yy}/\Gamma = 0.7$, for spin (c) up and (d) down. $G_{\sigma}^{<}$ and ρ_{σ}^r for consecutive bias voltages eV are shifted by a constant offset $a = 0.25$ for better visibility. The legend applies to all subplots.

between both GFs.

The conductance can be partitioned into two regimes: (i) $eV < T_K^{\text{eq}}$ and (ii) $eV > T_K^{\text{eq}}$ which are connected by a crossover regime. In both cases we consider the temperature being the smallest energy scale i. e. $T \ll T_K^{\text{eq}}, eV$. For bias voltages that are lower than T_K^{eq} , the system cross-over to a regime in which the impurity spin is screened and $U(1)$ symmetry is dynamically restored. As a consequence, the backscattered current vanishes even when the initial parameters break the $U(1)$ symmetry, implying that the total edge has a perfect zero-bias differential conductance.

For a setup with broken $U(1)$ symmetry, the equilibrium RG flow equations (25) are cut-off by $eV > T_K^{\text{eq}}$ [71, 72], therefore preventing the system from approaching the strong coupling fixed point and restoring the perfect edge. In the symmetric case, $\Delta J_{yy} = 0$, the fluctuation-dissipation theorem holds perfectly for each spin sector individually, and the conductance vanishes regardless of eV .

Numerically we find small negative values for I_B in the $eV < T_K^{\text{eq}}$ regime for broken symmetry that we trace back to three sources of errors. Firstly, the error increases with increasing the quench ΔJ_{yy} as a consequence of the discrete representation of the continuum problem by the Wilson chain [63, 73, 74]. Secondly, the smaller eV the smaller the difference between both GFs will be indicated in Fig. 3. Therefore, the relative error due to subtraction and integration is increasing. Thirdly, the linear conductance is proportional to V^{-1} requiring a high numerical precision of the integral determining I_B for small eV in Eq. (9). A voltage of order $eV/\Gamma \sim 10^{-3}$ demands a pre-

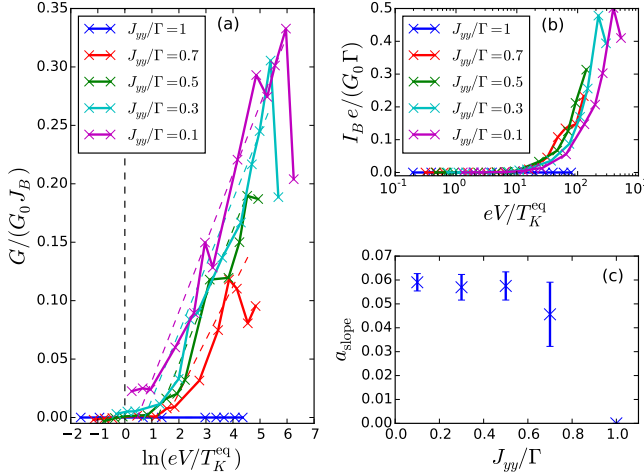


FIG. 4. (a) Linear conductivity $G = I_B/V$ as function of voltage eV/T_K^{eq} for different couplings J_{yy} . $I_B = 0$ for the $U(1)$ symmetric case $J_{yy} = \Gamma$. The vertical black dashed line indicates $eV = T_K^{\text{eq}}$. The other dashed lines represent the fits to Eq. (36). (b) Backscattering current I_B as function of eV/T_K^{eq} . (c) Slopes a_{slope} for the different fits in subplot (a). The error bars stem from the numerical fitting process. The values for T_K^{eq} are shown in Fig. 2(c). In all cases $J_{xx} = J_{zz} = \Gamma$.

cision of the backscattering current of at least four relevant digits. Here, not only the scattering states NRG but also the discretization of the spectral function on a finite frequency grid generates a small error in the numerical integration. We find that the smallest voltage, for which we could still get results that are not overshadowed by numerical noise, is $eV/\Gamma \approx 0.005$.

When we start in the large eV regime and decrease the voltage, the finite G for broken symmetry is also reduced until the system reaches the small eV regime. In the crossover regime, we extracted the parameter of a fitting function

$$G/J_B = a_{\text{slope}} \ln(eV/T_K^{\text{eq}}) + b \quad (36)$$

to the data shown in Fig. 4(a). The function is added as dashed lines in the same color to the plot. We find that the slope a_{slope} depicted in Fig. 4(c) is nearly independent of the coupling constant J_{yy} .

D. Finite backscattered current for $T > T_K^{\text{eq}}$

As in the previous section, we retain the parameters of a diagonal matrix $J_{\alpha\beta}$ with $J_{xx} = J_{zz} = \Gamma$ and use J_{yy} as a tuning parameter. The cut-off of the RG flow-equations does not necessarily have to come from high bias voltage but can be due to finite temperature as well. For the regime $eV < T_K^{\text{eq}} < T$, we expect that a setup with a broken $U(1)$ symmetry will not have its edge reconstructed and a finite backscattering will be observed. We choose

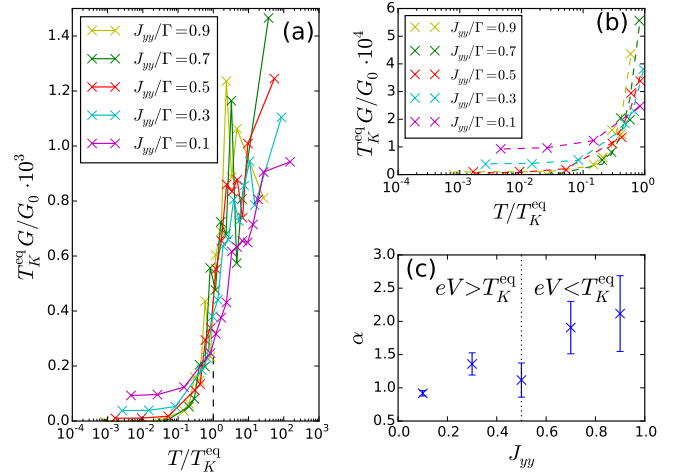


FIG. 5. (a) Linear conductivity G as function of temperature T/T_K^{eq} for a fixed $eV/\Gamma = 0.01$ and different couplings J_{yy} . The black dashed line indicates T_K^{eq} . Below $T/T_K^{\text{eq}} = 1$ the conductance $G \rightarrow 0$ when $eV < T_K^{\text{eq}}$ (yellow, green curve). The lines are a guide to the eye. (b) Power-law fit (Eq. (37)) to the data points (crosses) of (a) for $T/T_K^{\text{eq}} < 1$. (c) Exponent α of the power-law fit: $\alpha \rightarrow 2$ (Fermi-Liquid) for $eV < T_K^{\text{eq}}$. The error bars stem from the numerical fitting process.

a fixed voltage $eV/\Gamma = 0.01$ and calculate G as function of T for various couplings J_{yy} in the symmetry broken regime. Our particular choice partitions our results into two groups: for $J_{yy}/\Gamma \geq 0.7$, we find $T_K^{\text{eq}} > eV$ while the voltage is the largest energy scale for $J_{yy}/\Gamma \leq 0.3$. For $J_{yy}/\Gamma = 0.5$, Kondo temperature and voltage are almost equal and the system is located in the crossover regime.

In the first case, the low temperature conductance shows a universal behavior for $T < T_K^{\text{eq}}$ approaching asymptotically zero [Fig. 5 (a)], as discussed in the previous section. If eV is the largest energy scale, then the conductance converges towards a finite value for $T \rightarrow 0$. This asymptotic value increases monotonically with the ratio eV/T_K^{eq} (see Fig. 5 (a) cyan and magenta curve), i.e. the earlier the perturbative RG flow equations are cut off by eV .

The low temperature behavior of G is converged and, in case of $eV < T_K^{\text{eq}}$, is expected to follow a power-law. We use a fit of the form

$$T_K^{\text{eq}} G(T) = b(T/T_K^{\text{eq}})^\alpha + c \quad (37)$$

and determine the exponent $\alpha = 2$ from the data presented in Fig. 5(b) as depicted on the right side of Fig. 5(c). An exponent of $\alpha = 2$ is associated with single-particle backscattering, but as noted in previous studies [36, 43] the nature of the low-energy fixed-point Hamiltonian is strongly restricted by symmetry considerations, and cannot contain a single-particle backscattering term as such a term will break time-reversal symmetry. While maintaining time-reversal symmetry, the leading possible perturbation is a two-particles backscat-

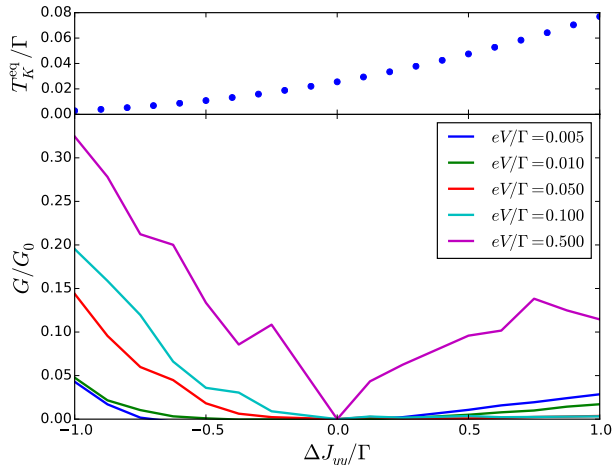


FIG. 6. Low temperature $G = I_B/V$ as a function of ΔJ_{yy} for different bias voltages eV and $T \rightarrow 0$. The upper subplot shows the corresponding equilibrium Kondo temperatures $T_K^{\text{eq}}(\Delta J_{yy})$.

tering term which should have a power-law corresponding to $\alpha = 4$. However, by applying finite voltage we, and any experimental setup, explicitly break time-reversal symmetry, and we understand the strong $\alpha = 2$ exponent to be a signature of non-equilibrium physics, with $G \propto (eVT)^2/T_K^4$. This suggests that for finite voltages the anisotropy might be the most dominant cause for the deviation from perfect conductance of the edge that was observed in experiments [5–24].

The offset c in Eq. (37) is numerically zero in the regime where $eV < T_K^{\text{eq}}$. In case eV is the relevant low-energy scale, it attains a nonzero value $c = c(eV/T_K^{\text{eq}})$, which is not constant and increases with eV .

E. Dynamical restoration of the $U(1)$ symmetry and the breakdown of backscattering current

Now we focus on the behavior of the conductance in the limit $T \rightarrow 0$ and finite eV as we break the $U(1)$ symmetry by a finite detuning $\Delta J_{yy} = \Gamma - J_{yy}$ and holding all other parameters fixed. The conductance vanishes at the symmetrical point $\Delta J_{yy} = 0$ ($J_{yy}/\Gamma = 1$) regardless of eV . The symmetric point is asymptotically restored by the Kondo effect in the limit $T \rightarrow 0$. Note, that the corresponding Kondo temperature $T_K^{\text{eq}} = T_K^{\text{eq}}(J_{yy})$ depends on the exchange coupling for otherwise fixed parameters. We calculate the conductance G as function of ΔJ_{yy} for a fixed bias voltage eV in the limit $T \rightarrow 0$ and plot the curve for different eV in Fig. 6. If $U(1)$ symmetry is broken, the conductance depends on the ratio eV/T_K^{eq} as discussed above.

When T_K^{eq} replaces eV as the largest low energy scale, the strong coupling fixed point is approached and backscattering is suppressed explaining the vanishing

conductance for $J_{yy}\Gamma < 1$ in Fig. 6. When $T_K^{\text{eq}} \approx eV$, a backscattering current is found as shown for large negative ΔJ_{yy} .

For $J_{yy}/\Gamma > 1$, T_K^{eq} is generally the largest energy scale except for $eV/\Gamma = 0.5$ (magenta curve) which still shows a significant backscattering conductance. The conductance is smaller than for $J_{yy}/\Gamma < 1$ due to the higher T_K^{eq} as the renormalization process is cut-off later and the system moves closer to a strong coupling fixed point. We find a finite conductance for large J_{yy} and $eV/\Gamma < 0.01$ albeit $eV < T_K^{\text{eq}}$. We again attribute this residual G to numerical inaccuracies in the calculation of the current via Eq. (9). The calculation of this residual G requires an accuracy of 5 digits at $eV/\Gamma < 0.01$ which is beyond our numerical precision. We conclude that $G \rightarrow 0$ for $eV/\Gamma < 0.01$. We believe that once eV exceeds 0.1Γ and eV of $O(T_K^{\text{eq}})$, the backscattering current emerges from the numerical noise in the regime $\Delta J_{yy} > 0$.

In short, we found a vanishing backscattering current at the symmetry point. The renormalization process is cut off for $eV > T_K^{\text{eq}}$, and a finite I_B remains for broken $U(1)$ symmetry.

V. SUMMARY AND DISCUSSION

In this paper we studied and analyzed the conductance of helical edge modes when coupled to a magnetic impurity, combining analytical and numerical methods. We derived a general expression for the non-equilibrium dc-current in Eq. (9) by coupling the helical edge electrons to localized levels. The current is independent of the specific details of the interactions of the local levels, which are encoded implicitly in the Green's functions for the localized levels. An analysis of the expression for the current using time-dependent gauge transformations as well as Hershfield's formalism revealed the role of a global $U(1)$ symmetry in protecting the perfect conductance of the helical modes. If the $U(1)$ symmetry is retained, then the edge manifests a perfect conductance even if time-reversal symmetry is broken. This conclusion was further corroborated by considering a specific exactly solvable interacting setup that maintains time-reversal symmetry but breaks $U(1)$ symmetry. We demonstrated in Eq. (31) that the conductance is not perfect even at zero-temperature and zero-bias. Similarly, the case where $U(1)$ symmetry was preserved but time-reversal symmetry broken was mapped onto an equilibrium setup with perfect conduction.

We then focused on an interaction Hamiltonian consisting of an exchange coupling between the levels and a localized impurity spin, defined by the coupling tensor $J_{\alpha,\beta}$ which allows for anisotropies that break the $U(1)$ symmetry. The one-loop RG flow equations of the exchange coupling, given in Eq. (25), showed that in general there is a dynamical process in which the $U(1)$ symmetry is restored. The equations flow to the strong-coupling fixed point, even when starting with symmetry

broken initial conditions. At low-temperatures and low-bias voltages the steady-state conductance approaches its quantized backscattering free value in the general case. This is a crossover transition, characterized by a scale T_K , below which the edge electrons tend to screen the impurity spin and form a Kondo singlet, isotropic by its nature.

However, the RG flow process in which the system crosses over to the low-energy isotropic regime can be cut-off before the system reaches the strong-coupling fixed point, either by the temperature or by the finite bias voltage. This leaves the impurity spin only partially screened and the system accumulates a finite correction to the quantized conductance. We studied the interplay between the anisotropy, temperature and bias voltage in the strongly-correlated regime numerically by employing the TD-NRG method. For $U(1)$ symmetry broken systems, with anisotropic exchange couplings, we found that if the temperature or bias voltage are larger than the Kondo scale, then there is a finite backscattering current, as the impurity is only fractionally screened. We tracked the crossover from the weak-coupling free-moment regime to the strong-coupling screened regime, characterized by a restored isotropic exchange and vanishing backscattered current. The perfect conductance of the edge is restored.

The challenging numerical analysis corroborates the analytical understanding of the role played by the global $U(1)$ symmetry in maintaining the conduction along the edge. Furthermore, it allowed us to extract the way in which the backscattering vanishes, and the perfect edge conductance is restored as we reduce the bias voltage (holding $T \ll T_K$) or reduce the temperature (holding $eV < T_K$). In the first case, the backscattering vanished logarithmically while $eV > T_K$, as it served as the effective cutoff for the RG process. In the latter case, when the temperature was reduced, the conductance follows a power-law $G \sim (T/T_K)^\alpha$ with an exponent of $\alpha = 2$, which is characteristic of a Fermi liquid fixed point. While such an exponent cannot characterize the linear-conductance, as it requires a time-reversal symmetry breaking term in the low-energy fixed point Hamiltonian, we understand it to be a feature of the nonequilibrium finite-bias condition that explicitly break this symmetry. We expect the term to scale with $(eVT)^2/T_K^4$, and intend to explore this further in future studies. The $\alpha = 2$ result suggests that the anisotropy might serve as a dominant cause for the experimental observation of non-perfect conductance in these setups.

ACKNOWLEDGMENTS

The authors would like to thank D. Litinski, A. Bruch, E. Sela, M. Goldstein, C. Karrasch, B. Sbierski, F. von Oppen and P. W. Brouwer for useful and enlightening discussions. YVA acknowledges funding from Deutsche Forschungsgemeinschaft (project C02 of CRC1283 and project A01 of CRC/TR183). F.B.A. and D.M. acknowl-

edge support from the Deutsche Forschungsgemeinschaft via project AN-275/8-1.

Appendix A: Poor man's scaling

Here, we analyze the low-energy scaling behavior of the Hamiltonian of Eqs. (21) and (23), for $\epsilon_d = U = 0$ and $S = 1/2$. To this end, we employ Anderson's poor man's scaling.

The model describes free fermions that couple to the impurity spin degrees of freedom with an effective Lorentzian density of states $\rho(\epsilon) = \rho_0/[1 + (\epsilon/\Gamma)^2]$. Around the weak-coupling point and for simplicity, we can replace the Lorentzian density of states with a hard-cutoff density of states of width 2Γ and $\rho_\Gamma = \pi\rho_0/2$, and ignore all the states that are outside this box. The width of the level Γ will now serve as the new high-energy cutoff. This can be thought of as a first step in a RG process where states which have small overlap with the impurity are being integrated out. While we know that for $U \neq 0$ the width Γ itself is a dynamic quantity that undergoes renormalization, we are working in the limit where $U = 0$ and are interested in the flow of the exchange coupling, therefore we can safely omit these high-energy modes.

The next step is to rescale the Hamiltonian and the field operators with the effective bandwidth $D \equiv \Gamma$

$$\begin{aligned} \frac{\mathcal{H}}{D} = & \sum_{\sigma} \int_{-1}^1 dx x \varphi_{\sigma}^{\dagger}(x) \varphi(x) + \\ & \sum_{\alpha, \beta, \lambda, \lambda'} J'_{\alpha, \beta} \int_{-1}^1 dx_1 dx_2 \varphi_{\lambda}^{\dagger}(x_1) \varphi_{\lambda'}(x_2) \sigma_{\lambda, \lambda'}^{\alpha} S^{\beta} \end{aligned} \quad (\text{A1})$$

where $J'_{\alpha, \beta} = J_{\alpha, \beta}/v_F$, and we have defined the dimensionless field operators

$$\varphi_{\sigma}(x) = \sqrt{D} \psi_{\sigma}(xD), \quad (\text{A2})$$

with $\psi_{\sigma}(\epsilon)$ the on-shell energy-field operator

$$\psi_{\sigma}(\epsilon) = \sqrt{\frac{D}{2}} \sum_k \gamma_{\sigma, k} \delta(\epsilon - \sigma \epsilon_k). \quad (\text{A3})$$

The next step is to divide the energy band into low-energy $|x| < 1 - dl$ and high-energy $1 - dl < |x| \leq 1$ modes, and integrate out the fast energy modes by perturbation theory. The leading order then gives

$$\begin{aligned} V_{\text{eff}} = & - \sum_{\{\lambda_i\}, \{\alpha_i\}, \{\beta_i\}} J_{\alpha_1, \beta_2} J_{\alpha_2, \beta_2} \sigma_{\lambda_1, \lambda_2}^{\alpha_1} \sigma_{\lambda_3, \lambda_4}^{\alpha_2} S^{\beta_1} S^{\beta_2} \times \\ & \int_{-1+dl}^{1-dl} dx_{1, <} dx_{2, <} \langle \varphi_{\lambda_1}^{\dagger}(x_{1, <}) \varphi_{\lambda_4}(x_{2, <}) \times \\ & \int_{1-dl}^1 dx_{1, >} dx_{2, >} \langle \varphi_{\lambda_2}(x_{>}) \varphi_{\lambda_3}^{\dagger}(x_{>}) \rangle \end{aligned} \quad (\text{A4})$$

and its corresponding contributions from the modes in $(-1, -1 + dl)$. We employ the identity

$$(\mathbf{A} \cdot \mathbf{S})(\mathbf{B} \cdot \mathbf{S}) = i(\mathbf{A} \times \mathbf{B}) \cdot \mathbf{S} + \mathbf{A} \cdot \mathbf{B} \quad (\text{A5})$$

to carry out the multiplications and arrive at

$$V_{\text{eff}} = 2dl \sum_{\{\alpha_i\}, \{\beta_i\}, \lambda_1 \lambda_2} \epsilon_{\alpha_1, \alpha_2, \alpha_3} \epsilon_{\beta_1, \beta_2, \beta_3} \times \\ J'_{\alpha_1, \beta_1} J'_{\alpha_2, \beta_2} \sigma_{\lambda_1, \lambda_2}^{\alpha_3} S^{\beta_3} \times \\ \int_{-1+dl}^{1-dl} dx_1, < dx_2, < \varphi_{\lambda_1}^\dagger(x_{1, <}) \varphi_{\lambda_1}(x_{2, <}), \quad (\text{A6})$$

where we have omitted constant terms and terms contributing to a scattering potential, which are irrelevant. The above expression can be written in a more concise form if we write the exchange couplings as vectors in the impurity spin-basis, $\mathbf{J}'_{\alpha} = \sum_{\beta} J'_{\alpha, \beta} \hat{\beta}$. We then write the effective Hamiltonian

$$\frac{\mathcal{H}'}{D} = \sum_{\sigma} \int_{-1+dl}^{1-dl} dx x \varphi_{\sigma}^\dagger(x) \varphi(x) + \\ \sum_{\{\alpha_i\}, \lambda, \lambda'} [\mathbf{J}'_{\alpha_1} + 2dl \epsilon_{\alpha_1, \alpha_2, \alpha_3} (\mathbf{J}'_{\alpha_2} \times \mathbf{J}'_{\alpha_3})] \cdot \mathbf{S} \\ \times \int_{-1+dl}^{1-dl} dx_1 dx_2 \varphi_{\lambda}^\dagger(x_1) \varphi_{\lambda'}(x_2) \sigma_{\lambda, \lambda'}^{\alpha_1}. \quad (\text{A7})$$

Finally, we rescale by $dx \rightarrow (1 - dl)^{1/2} dx$, and write \mathcal{H}' in terms of $D' = (1 - dl)D$, to have

$$\frac{\mathcal{H}'}{D'} = \sum_{\sigma} \int_{-1}^1 dx x \varphi_{\sigma}^\dagger(x) \varphi(x) + \\ \sum_{\{\alpha_i\}, \lambda, \lambda'} [\mathbf{J}'_{\alpha_1} + 2dl \epsilon_{\alpha_1, \alpha_2, \alpha_3} (\mathbf{J}'_{\alpha_2} \times \mathbf{J}'_{\alpha_3})] \cdot \mathbf{S} \\ \times \int_{-1}^1 dx_1 dx_2 \varphi_{\lambda}^\dagger(x_1) \varphi_{\lambda'}(x_2) \sigma_{\lambda, \lambda'}^{\alpha_1}. \quad (\text{A8})$$

We therefore arrive at the following renormalization group flow equations

$$\frac{d\mathbf{J}_i}{dl} = 2\pi\rho_{\Gamma} \sum_{j,k} \epsilon_{i,j,k} \mathbf{J}_j \times \mathbf{J}_k, \quad (\text{A9})$$

with the dimensions restored, and we took the relation $\rho = (2\pi v_F)^{-1}$ for a flat band. A detailed analysis of this RG equations can be found in the appendix in Ref. ([60])

-
- [1] B. A. Bernevig, T. L. Hughes, and S.-C. Zhang, *Science* **314**, 1757 (2006).
- [2] C. L. Kane and E. J. Mele, *Phys. Rev. Lett.* **95**, 146802 (2005).
- [3] X.-L. Qi and S.-C. Zhang, *Rev. Mod. Phys.* **83**, 1057 (2011).
- [4] M. Z. Hasan and C. L. Kane, *Rev. Mod. Phys.* **82**, 3045 (2010).
- [5] Z.-Y. Jia, Y.-H. Song, X.-B. Li, K. Ran, P. Lu, H.-J. Zheng, X.-Y. Zhu, Z.-Q. Shi, J. Sun, J. Wen, D. Xing, and S.-C. Li, *Phys. Rev. B* **96**, 041108(R) (2017).
- [6] Z. Fei, T. Palomaki, S. Wu, W. Zhao, X. Cai, B. Sun, P. Nguyen, J. Finney, X. Xu, and D. H. Cobden, *Nature Physics* **13**, 677 (2017).
- [7] C. Sabater, D. Gosálbez-Martínez, J. Fernández-Rossier, J. G. Rodrigo, C. Untiedt, and J. J. Palacios, *Phys. Rev. Lett.* **110**, 176802 (2013).
- [8] S. Mueller, A. N. Pal, M. Karalic, T. Tschirky, C. Charpentier, W. Wegscheider, K. Ensslin, and T. Ihn, *Phys. Rev. B* **92**, 081303(R) (2015).
- [9] T. Li, P. Wang, G. Sullivan, X. Lin, and R.-R. Du, *Phys. Rev. B* **96**, 241406(R) (2017).
- [10] K. Suzuki, Y. Harada, K. Onomitsu, and K. Muraki, *Phys. Rev. B* **91**, 245309 (2015).
- [11] L. Du, I. Knez, G. Sullivan, and R.-R. Du, *Phys. Rev. Lett.* **114**, 096802 (2015).
- [12] E. M. Spanton, K. C. Nowack, L. Du, G. Sullivan, R.-R. Du, and K. A. Moler, *Phys. Rev. Lett.* **113**, 026804 (2014).
- [13] K. Suzuki, Y. Harada, K. Onomitsu, and K. Muraki, *Phys. Rev. B* **87**, 235311 (2013).
- [14] E. B. Olshanetsky, Z. D. Kvon, G. M. Gusev, A. D. Levin, O. E. Raichev, N. N. Mikhailov, and S. A. Dvoretzky, *Phys. Rev. Lett.* **114**, 126802 (2015).
- [15] I. Knez, R.-R. Du, and G. Sullivan, *Phys. Rev. Lett.* **107**, 136603 (2011).
- [16] G. M. Gusev, E. B. Olshanetsky, Z. D. Kvon, O. E. Raichev, N. N. Mikhailov, and S. A. Dvoretzky, *Phys. Rev. B* **88**, 195305 (2013).
- [17] G. M. Gusev, Z. D. Kvon, E. B. Olshanetsky, A. D. Levin, Y. Krupko, J. C. Portal, N. N. Mikhailov, and S. A. Dvoretzky, *Phys. Rev. B* **89**, 125305 (2014).
- [18] G. M. Gusev, Z. D. Kvon, O. A. Shegai, N. N. Mikhailov, S. A. Dvoretzky, and J. C. Portal, *Phys. Rev. B* **84**, 121302(R) (2011).
- [19] G. Grabecki, J. Wróbel, M. Czapkiewicz, L. Cywiński, S. Gieraltowska, E. Guziewicz, M. Zholudev, V. Gavrilenko, N. N. Mikhailov, S. A. Dvoretzky, F. Teppe, W. Knap, and T. Dietl, *Phys. Rev. B* **88**, 165309 (2013).
- [20] K. C. Nowack, E. M. Spanton, M. Baenninger, M. Knig, J. R. Kirtley, B. Kalisky, C. Ames, P. Leubner, C. Brne, H. Buhmann, L. W. Molenkamp, D. Goldhaber-Gordon, and K. A. Moler, *Nature Materials* **12**, 787 (2013).
- [21] A. Kononov, S. V. Egorov, Z. D. Kvon, N. N. Mikhailov, S. A. Dvoretzky, and E. V. Deviatov, *JETP Letters* **101**, 814 (2015).
- [22] C. Brüne, A. Roth, H. Buhmann, E. M. Hankiewicz, L. W. Molenkamp, J. Maciejko, X.-L. Qi, and S.-C. Zhang, *Nature Physics* **8**, 485 (2012).

- [23] A. Roth, C. Brüne, H. Buhmann, L. W. Molenkamp, J. Maciejko, X.-L. Qi, and S.-C. Zhang, *Science* **325**, 294 (2009).
- [24] M. König, S. Wiedmann, C. Brüne, A. Roth, H. Buhmann, L. W. Molenkamp, X.-L. Qi, and S.-C. Zhang, *Science* **318**, 766 (2007).
- [25] C. Xu and J. E. Moore, *Phys. Rev. B* **73**, 045322 (2006).
- [26] A. Ström, H. Johannesson, and G. I. Japaridze, *Phys. Rev. Lett.* **104**, 256804 (2010).
- [27] T. L. Schmidt, S. Rachel, F. von Oppen, and L. I. Glazman, *Phys. Rev. Lett.* **108**, 156402 (2012).
- [28] N. Kainaris, I. V. Gornyi, S. T. Carr, and A. D. Mirlin, *Phys. Rev. B* **90**, 075118 (2014).
- [29] J. I. Väyrynen, D. I. Pikulin, and J. Alicea, *Phys. Rev. Lett.* **121**, 106601 (2018).
- [30] J. I. Väyrynen, M. Goldstein, and L. I. Glazman, *Phys. Rev. Lett.* **110**, 216402 (2013).
- [31] A. Rod, T. L. Schmidt, and S. Rachel, *Phys. Rev. B* **91**, 245112 (2015).
- [32] P. P. Aseev and K. E. Nagaev, *Phys. Rev. B* **94**, 045425 (2016).
- [33] J. Wang, Y. Meir, and Y. Gefen, *Phys. Rev. Lett.* **118**, 046801 (2017).
- [34] C.-H. Hsu, P. Stano, J. Klinovaja, and D. Loss, *Phys. Rev. B* **96**, 081405(R) (2017).
- [35] C.-H. Hsu, P. Stano, J. Klinovaja, and D. Loss, *Phys. Rev. B* **97**, 125432 (2018).
- [36] N. Lezmy, Y. Oreg, and M. Berkooz, *Phys. Rev. B* **85**, 235304 (2012).
- [37] E. Eriksson, A. Ström, G. Sharma, and H. Johannesson, *Phys. Rev. B* **86**, 161103 (2012).
- [38] B. L. Altshuler, I. L. Aleiner, and V. I. Yudson, *Phys. Rev. Lett.* **111**, 086401 (2013).
- [39] K. Hattori and A. Rosch, *Phys. Rev. B* **90**, 115103 (2014).
- [40] O. M. Yevtushenko, A. Wugalter, V. I. Yudson, and B. L. Altshuler, *EPL (Europhysics Letters)* **112**, 57003 (2015).
- [41] J. I. Väyrynen, F. Geissler, and L. I. Glazman, *Phys. Rev. B* **93**, 241301(R) (2016).
- [42] O. M. Yevtushenko and V. I. Yudson, *Phys. Rev. Lett.* **120**, 147201 (2018).
- [43] J. I. Väyrynen, M. Goldstein, Y. Gefen, and L. I. Glazman, *Phys. Rev. B* **90**, 115309 (2014).
- [44] J. Maciejko, C. Liu, Y. Oreg, X.-L. Qi, C. Wu, and S.-C. Zhang, *Phys. Rev. Lett.* **102**, 256803 (2009).
- [45] J. Maciejko, *Phys. Rev. B* **85**, 245108 (2012).
- [46] V. Cheianov and L. I. Glazman, *Phys. Rev. Lett.* **110**, 206803 (2013).
- [47] L. Kimme, B. Rosenow, and A. Brataas, *Phys. Rev. B* **93**, 081301(R) (2016).
- [48] P. D. Kurilovich, V. D. Kurilovich, I. S. Burmistrov, and M. Goldstein, *JETP Letters* **106**, 593 (2017).
- [49] V. D. Kurilovich, P. D. Kurilovich, and I. S. Burmistrov, *Phys. Rev. B* **95**, 115430 (2017).
- [50] V. D. Kurilovich, P. D. Kurilovich, I. S. Burmistrov, and M. Goldstein, *Phys. Rev. B* **99**, 085407 (2019).
- [51] C. Wu, B. A. Bernevig, and S.-C. Zhang, *Phys. Rev. Lett.* **96**, 106401 (2006).
- [52] Y. Tanaka, A. Furusaki, and K. A. Matveev, *Phys. Rev. Lett.* **106**, 236402 (2011).
- [53] R. Bulla, T. A. Costi, and T. Pruschke, *Rev. Mod. Phys.* **80**, 395 (2008).
- [54] M. G. Pala, M. Governale, U. Zülicke, and G. Iannaccone, *Phys. Rev. B* **71**, 115306 (2005).
- [55] Y. Meir and N. S. Wingreen, *Phys. Rev. Lett.* **68**, 2512 (1992).
- [56] D. C. Langreth, *Linear and Nonlinear Electron Transport in Solids*, edited by J. T. Devreese and V. E. van Doren, Nato Advanced Study Institute, Series B: Physics (Plenum Press, New York, 1976).
- [57] K. Kang, S. Y. Cho, J.-J. Kim, and S.-C. Shin, *Phys. Rev. B* **63**, 113304 (2001).
- [58] S. Hershfield, *Phys. Rev. Lett.* **70**, 2134 (1993).
- [59] E. Lebanon, A. Schiller, and F. B. Anders, *Phys. Rev. B* **68**, 155301 (2003).
- [60] Y. Vinkler-Aviv, P. W. Brouwer, and F. von Oppen, *Phys. Rev. B* **96**, 195421 (2017).
- [61] K. G. Wilson, *Rev. Mod. Phys.* **47**, 773 (1975).
- [62] F. B. Anders and A. Schiller, *Phys. Rev. Lett.* **95**, 196801 (2005).
- [63] F. B. Anders and A. Schiller, *Phys. Rev. B* **74**, 245113 (2006).
- [64] F. B. Anders, *Phys. Rev. Lett.* **101**, 066804 (2008).
- [65] F. B. Anders and S. Schmitt, *Journal of Physics: Conference Series* **220**, 012021 (2010).
- [66] W. C. Oliveira and L. N. Oliveira, *Phys. Rev. B* **49**, 11986 (1994).
- [67] R. Peters, T. Pruschke, and F. B. Anders, *Phys. Rev. B* **74**, 245114 (2006).
- [68] A. Weichselbaum and J. von Delft, *Phys. Rev. Lett.* **99**, 076402 (2007).
- [69] F. B. Anders, *Journal of Physics: Condensed Matter* **20**, 195216 (2008).
- [70] R. Bulla, A. C. Hewson, and T. Pruschke, *Journal of Physics: Condensed Matter* **10**, 8365 (1998).
- [71] L. Borda and A. Zawadowski, *Phys. Rev. B* **81**, 153303 (2010).
- [72] A. Rosch, J. Kroha, and P. Wölfle, *Phys. Rev. Lett.* **87**, 156802 (2001).
- [73] E. Eidelstein, A. Schiller, F. Güttge, and F. B. Anders, *Phys. Rev. B* **85**, 075118 (2012).
- [74] F. Güttge, F. B. Anders, U. Schollwock, E. Eidelstein, and A. Schiller, *Phys. Rev. B* **87**, 115115 (2013).
- [75] A. C. Hewson, *The Kondo Problem to Heavy Fermions* (Cambridge University Press, Cambridge, 1993).